Disordered $Gd_6UO_{12-\delta}$ with the cation antisite defects prepared by a combined mechanochemical−thermal method

G. Darin[a], K. Imakuma[a], R.T. Santiago[b], K.L. Da Silva[b,c,d,*], L.F. Cótica[b], M. Fabián[c], J. Valíček[e,f], H. Hahn[d], V. Šepelák[c,d,e]

[a] Nuclear and Energy Research Institute, IPEN/CNEN-SP, 05508-000 São Paulo, Brazil
[b] Physics Department, State University of Maringá, 87020-900 Maringá, Brazil
[c] Institute of Geotechnics, Slovak Academy of Sciences, 04001, Košice, Slovakia
[d] Institute of Nanotechnology, Karlsruhe Institute of Technology, 76344, Eggenstein-Leopoldshafen, Germany
[e] Faculty of Technology, College of Technology and Business in České Budějovice, 37001 České Budějovice, Czech Republic
[f] Faculty of Engineering, Slovak University of Agriculture, 94976 Nitra, Slovakia

A B S T R A C T

The synthesis of the rhombohedral $Gd_6UO_{12-\delta}$ is reported via mechanochemical processing of stoichiometric Gd_2O_3/UO_2 mixtures and their subsequent annealing. Rietveld refinement of XRD data reveals that the as-prepared material exhibits a remarkable degree of cation antisite disorder and oxygen deficiency. The simulations of intensities of the selected XRD superlattice reflections are performed for limiting states of $Gd_6UO_{12-\delta}$ with its most extreme degrees of the cation antisite disorder. On the basis of the estimated bond lengths it can be stated that distorted geometry of structural units in the material is a consequence of its relatively large oxygen deficiency.

There is continuous interest in gadolinium uranate, Gd_6UO_{12}, because of its applications, such as material for nuclear fuel forms and nuclear waste immobilization [1]. Gd_6UO_{12} crystallizes in a rhombohedral form, which is related to the fluorite-type structure with space group R-3 [2,3]. The material incorporates Gd^{3+} cations occupying the general 18f sites (Wyckoff notation) with seven-fold coordination of oxygen ions, and U^{6+} cations occupying 3a sites with octahedral coordination [4,5]. Correspondingly, the structural formula of this compound in *equilibrium (ordered) state*, emphasizing the site occupancy at the atomic level, may be written as $\{Gd_6\}_{18f}[U]_{3a}O_{12}$. Note that despite its deceptively simple structure, Gd_6UO_{12} exhibits complex disordering phenomena involving the cation antisite defects and anion vacancies randomly distributed over the sites. In this case, the formula of the material may be expressed as $\{Gd_{6-\beta}U_\beta\}_{18f}[U_{1-\beta}Gd_\beta]_{3a}O_{12-\delta}$. Here, the symbol β represents the fraction of uranium cations located at 18f sites and δ is *the oxygen deficiency parameter*. In the fully disordered rhombohedral state with the random distribution of cations ($\beta = 6/7$), the structural formula of the material may be written as $\{Gd_{36/7}U_{6/7}\}_{18f}[U_{1/7}Gd_{6/7}]_{3a}O_{12-\delta}$. Note that this state is entirely hypothetical one representing the cation configuration with the maximum configurational entropy. As a result of the formation of the cation antisite defects and anion Frenkel defects, the rhombohedral symmetry of the ordered Gd_6UO_{12} phase evolves in favor of cubic symmetry which is referred as a disordered fluorite phase [4,6].

It is widely appreciated that the performance of Gd_6UO_{12} is closely related to the ways in which it is processed. The conventional multi-steps solid state synthesis of this material involves heating of pressed pellets of reactants (*e.g.*, Gd_2O_3 and UO_2) at temperatures above 1700 K in air for a long period (sometimes many days), followed by grinding, repelletising and further prolonged resintering, and, finally, slow cooling to room temperature lasting several days [4,7–10]. Various wet (solution) chemistry-based multi-steps routes involving a combustion method have also been developed to synthesize Gd_6UO_{12} [1,3,11–14]. However, most of the solution chemistry-based routes still involve calcinations, although at relatively lower temperatures. Moreover, a large amount of gases evolved during the combustion reaction can leads to the formation of a highly porous product rather than compacted one. Fortunately, such hurdles can be overcome by chemical reactions initiated or accelerated by means of mechanical force [15]. Mechanically induced chemistry (the so-called *mechanochemistry*) has recently been identified by IUPAC as one of the top ten emerging

* Corresponding author.
E-mail address: lucenildodasilva@yahoo.com.br (K.L. Da Silva).

technologies in chemistry providing an efficient and facile access to various materials [16].

In the present work, for the first time, the synthesis of $Gd_6UO_{12-\delta}$ is reported via mechanochemical processing of stoichiometric Gd_2O_3/UO_2 mixtures and their subsequent annealing at moderate temperatures. The combined mechanochemical–thermal process used here represents an effective, solvent-free, and high-yield procedure for the synthesis of this nuclear material. On the basis of the Rietveld analysis of X-ray diffraction (XRD) data, precise information on the unit cell dimensions, atomic positional parameters, the occupation factors and bond lengths in the investigated system are obtained. It is demonstrated that the as-prepared material exhibits a remarkable cation antisite disorder and oxygen deficiency. Moreover, unusual local six-fold coordination of Gd^{3+} cations located at the 18f sites is revealed. For the first time, quantitative information on the degree of cation antisite disorder is derived from the Rietveld refinement.

The overall chemical reaction leading to the formation of Gd_6UO_{12} can be written as $3Gd_2O_3 + UO_2 + \frac{1}{2}O_2 \rightarrow Gd_6UO_{12}$. At first, the stoichiometric mixture of UO_2 (produced by Nuclear Materials Laboratory at the Industrial Nuclear Center of Aramar, São Paulo, Brazil) and Gd_2O_3 (Alfa Aesar) was preactivated by ball-milling in a Pulverisette 6 mill (Fritsch, Germany) for 12 hours at 300 rpm in N_2 atmosphere. A grinding chamber and balls made of stainless steel were used. The ball-to-powder weight ratio was 11:1. The mixture of mechanically treated precursors was pressed into pellets at 390 MPa, which were subsequently heated for 3 hours at 1573 K in air. XRD patterns of powdered samples were taken in the range from 10° to 80° (2Θ) (with angular step of 0.02°) using Cu Kα radiation and a C1702 diffractometer (Shimadzu, Japan) operating in Bragg-Brentano configuration. The Rietveld refinement of XRD data was performed using the *FullProf Suite* software [17]. In the refinement, the individual occupancies of Gd and U ions on 3a and 18f sites were left to freely vary, whereas the occupation factors of O^{2-} anions were fixed. It is because the atomic scattering factor of oxygen is considerably lower than that of heavy Gd and U atoms [18]. The oxygen deficiency parameter (δ) is calculated using the refined occupation factors of Gd and U ions under the constraint of the charge neutrality of the system. The *degree of the cation antisite disorder* was calculated using the refined occupancy of uranium cations on 18f sites, β, according to formula ASD $= (\beta - \beta_o)/(\beta_d - \beta_o)$, where β_o and β_d represent the occupancies of uranium cations on 18f sites in the fully ordered ($\beta_o = 0$) and fully disordered Gd_6UO_{12} with the random distribution of cations ($\beta_d = 6/7$), respectively. The degree of the long-range disorder (DOD) in $Gd_6UO_{12-\delta}$ was also calculated using the Warren's method [19]. The ICSD database [20] was utilized for phase identification. The 3-dimmensional structure of the as-prepared material was visualized using the *Vesta* program [21].

The XRD pattern of the mechanically preactivated $3Gd_2O_3 + UO_2$ mixture after its subsequent annealing at 1573 K for 3 hours, refined using the Rietveld method, is shown in Fig. 1. The pattern is well-fitted using a single rhombohedral phase (ICSD collection code 21945) with space group R-3 [20]. No spurious or minority phases have been observed. It clearly demonstrates that the combined mechanochemical–thermal treatment of the precursors leads to the formation of the desired gadolinium uranate phase with the phase purity of 100%. Such a favorable formation of the uranate is a consequence of an accelerated mass transfer and enhanced ionic diffusivity at contact zones between precursors due to reduced diffusion paths as a result of their mechanical preactivation and the partial mechanosynthesis of the target phase [15] (see Fig. 1 in related Data in Brief). It should be emphasized that the same thermal processing of the non-milled mixture does not lead to the complete transformation of educts to the final Gd_6UO_{12} phase. The latter is also supported by the
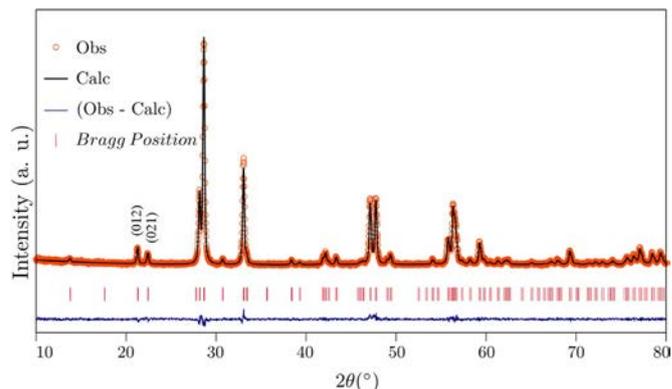
Fig. 1. The refined XRD pattern of $Gd_6UO_{12-\delta}$ prepared by the mechanochemical–thermal route. Miller indices denote two superlattice reflections used for simulations of peak intensities of $Gd_6UO_{12-\delta}$ with various β and δ parameters.
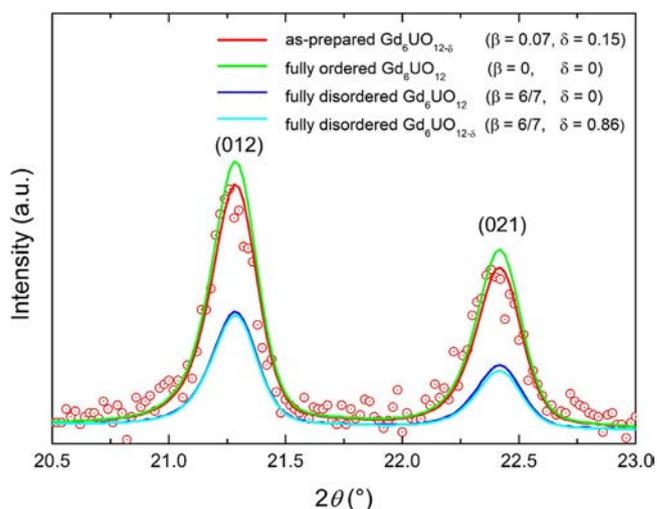
Fig. 2. The XRD superlattice (012) and (021) reflections for $Gd_6UO_{12-\delta}$ with various β and δ parameters characterizing the various degree of cation antisite disorder and oxygen deficiency, respectively. The simulated diffraction patterns are represented by solid lines. Open circles are the measured diffraction data of the as-prepared $Gd_6UO_{12-\delta}$.

results of thermal analysis given in related Data in Brief (see Fig. 2 and Fig. 3).

The derived crystal structure parameters of the as-prepared phase are listed in Table 1. The lattice parameters of the rhombohedral structure of the product ($a = 10.089(5)$ Å, $c = 9.517(5)$ Å) are in good agreement with those reported previously [1,3,8]. An important observation is that the mechanochemical–thermal processing leads to the formation of structure with both the cation antisite defects ($\beta = 0.0700(7)$) and anion vacancies ($\delta = 0.149(50)$), namely, to the nonequilibrium disordered and oxygen-deficient $\{Gd_{5.930}U_{0.070}\}_{18f}[U_{0.917}Gd_{0.066}]_{3a}O_{11.851}$ phase. The degree of the cation antisite disorder in the rhombohedral product phase is found to be ASD $= 0.0817(8)$. It should be emphasized that the nonequilibrium distribution of cations within distorted polyhedra has also been reported for other oxide structures (*e.g.*, spinel, olivine, and mullite) prepared by nonconventional mechanochemical routes [22–25]. The degree of the long-range disorder in $Gd_6UO_{12-\delta}$ is found to be DOD $= 0.129(22)$ that is slightly higher than the derived value of ASD. Note that the DOD reflects the distorted geometry of octahedra around the 18f site discussed below.

It is well known that high-energy milling induces a variety of transformations and reactions in oxides such as disordering and

Table 1
Crystal structure parameters (a, c, V), atomic positions (x, y, z), occupation factors (occ), and interatomic distances derived from the Rietveld analysis of XRD data of the as-prepared $Gd_6UO_{12-\delta}$. S is the degree of the long-range order. The fixed parameters are indicated by asterisk.

empirical formula	$\{Gd^{3+}_{5.930}U^{4+}_{0.070}\}_{18f}[U^{6+}_{0.883}U^{4+}_{0.034}Gd^{3+}_{0.066}]_{3a}O_{11.851}$				
crystal system	rhombohedral				
space group	R-3				
a (Å)	10.089(5)				
c (Å)	9.517(5)				
V (Å^3)	839.014(70)				
δ (oxygen deficiency)	0.149(50)				
atomic position	x	y	z	occ	rel. occ (%)
$[U^{6+}]_{3a}$	0.00000(0)	0.00000(0)	0.00000(0)	0.883(10)	0.883(10)
$[U^{4+}]_{3a}$	0.00000(0)	0.00000(0)	0.00000(0)	0.034(10)	0.034(10)
$[Gd]_{3a}$	0.00000(0)	0.00000(0)	0.00000(0)	0.066(10)	0.066(10)
$\{Gd\}_{18f}$	0.12273(19)	0.41612(24)	0.02094(17)	5.930(70)	0.988(12)
$\{U^{4+}\}_{18f}$	0.12273(19)	0.41612(24)	0.02094(17)	0.0700(7)	0.0120(1)
$\{O_1\}_{18f}$	0.19273(198)	0.03192(312)	0.11563(133)	6.000*	1.000*
$\{O_2\}_{18f}$	0.14650(247)	0.45139(200)	0.26908(150)	6.000*	1.000*
goodness parameters: R_p, R_{wp}; χ^2	7.77%, 10.3%; 1.31				
M–O bond distance for site $3a$ (Å)	M–O bond distance for site $18f$ (Å)				
$[U,Gd]_{3a}$–O 2.11(3)	$\{Gd,U\}_{18f}$–O 2.34(1)				
$[U,Gd]_{3a}$–O 2.11(3)	$\{Gd,U\}_{18f}$–O 2.20(3)				
$[U,Gd]_{3a}$–O 2.11(3)	$\{Gd,U\}_{18f}$–O 2.42(4)				
$[U,Gd]_{3a}$–O 2.11(3)	$\{Gd,U\}_{18f}$–O 2.38(2)				
$[U,Gd]_{3a}$–O 2.11(3)	$\{Gd,U\}_{18f}$–O 2.35(2)				
$[U,Gd]_{3a}$–O 2.11(3)	$\{Gd,U\}_{18f}$–O 2.31(3)				
DOD = $1 - S = 1 - ($rel. occ $[U]_{3a}$ + rel. occ $\{Gd\}_{18f} - 1) = 0.129(22)$					
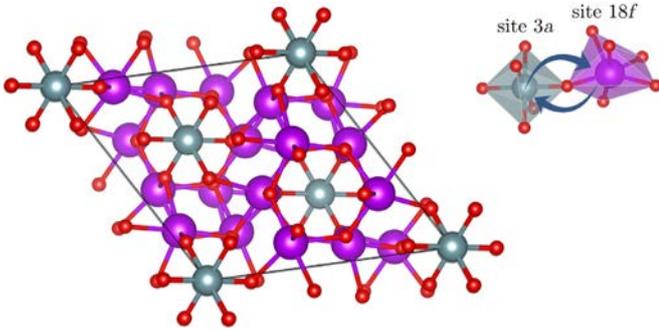
Fig. 3. The rhombohedral crystal structure of $Gd_6UO_{12-\delta}$. The mechanochemical–thermal route leads to the formation of structure with both the cation antisite defects and anion vacancies. The crystal-chemical formula of the as-prepared material, emphasizing its nonequilibrium cation distribution, can be written as $\{Gd_{5.930}U_{0.070}\}_{18f}[U_{0.917}Gd_{0.066}]_{3a}O_{11.851}$. The arrows indicate the distribution of cations over the $3a$ and $18f$ sites of octahedral coordination with the symmetrical and distorted geometry, respectively.

amorphization (including surface amorphization), grain boundary disordering, polymorphic transformations, etc. [15]. It also creates defects, some being specific to oxides, such as Schottky or Frenkel defects or crystallographic shear planes (Wadsley defects) [26]. In general, the nature of disorder in oxides prepared by mechanochemical routes includes, e.g., (i) a nonequilibrium distribution of cations over non-equivalent cation sublattices provided by a complex oxide structure (the so-called cation antisite disorder), (ii) a canted spin arrangements in the case of magnetic compounds, (iii) distorted geometry of constitutive polyhedra, and (iv) a defective cation centers with an unsaturated oxygen coordination in the near-surface layers of oxide nanoparticles [15]. In line with these general disordering features, we demonstrate that the as-prepared $Gd_6UO_{12-\delta}$ phase exhibits a remarkable cation antisite disorder with a relatively high concentration of oxygen vacancies and distorted octahedra around the $18f$ sites (see below).

The mechanically induced structural disorder in oxides is spatially confined to their interfacial nanosized regions (the so-called nanodomains) [15]. For example, disordered spinel oxides exhibit non-uniform structure; the atomic configurations in the interface/surface regions of nanooxides are chiefly characterized by a nearly random arrangement of cations, whereas the ordered grains exhibit an equilibrium cation distribution. Taking into account the microcrystalline (not nanostructured) nature of the as-prepared $Gd_6UO_{12-\delta}$ phase, we exclude the presence of such nanodomains in the sample.

It is well known that the change in cation disorder in solids is usually induced by high temperature [27], high pressure [28], irradiation of a material with high-energy electrons, ions or neutrons [29], and its particle size reduction to the nanoscale range [30]. Independently of the ionic configuration in materials, all these processing parameters were found to change the cation distribution in solids towards the random arrangement [15]. A radiation-induced order–to–disorder phase transformation has already been observed in Gd_6UO_{12} by Tang et al. [4,9,10]. With increasing dose of the ion irradiation, the material was found to be transformed from an ordered rhombohedral to a disordered rhombohedral phase and even to a cubic fluorite structure. This transformation is, according to Tang et al. [4,9,10], accompanied by the disappearance of the XRD peaks associated with the fluorite structural derivative (the so-called superlattice reflections). However, these authors have not provided quantitative information on the increasing ASD with increasing radiation dose.

To reveal impact of ASD on the intensities of superlattice reflections and to support the present quantitative results derived from Rietveld analysis, we perform simulations of the selected superlattice reflections for $Gd_6UO_{12-\delta}$ with various β and δ parameters. The two superlattice reflections with Miller indices (012) and (021) are used for simulations because they are not overlapping with a good signal-to-noise ratio, see Fig. 1. It is revealed that the intensity of these Bragg peaks is the highest for the fully ordered Gd_6UO_{12} ($\beta_o = 0$; i.e., ASD = 0), where all Gd and U atoms occupy $18f$ and $3a$ positions, respectively; see Fig. 2. The intensity of superlattice reflections is found to decrease with increasing ASD and δ. For a fictitious case of the fully disordered rhombohedral Gd_6UO_{12} phase ($\beta_d = 6/7$; i.e., ASD = 1) the intensity of superlattice reflections reaches about 40% of the peak intensity of the fully ordered state. For the as-prepared $Gd_6UO_{12-\delta}$, the relative intensity of superlattice reflections is about 90%. Within the interval $0 \leq \delta \leq 0.86$, the oxygen deficiency has only a minor influence on

Table 2
The relative intensity (I) of superlattice reflections with Miller indices (012) and (021) for $Gd_6UO_{12-\delta}$ with various β and δ parameters.

Fraction of uranium cations on 18f sites, β	Degree of the cation antisite disorder, ASD	Oxygen deficiency parameter, δ	Type of structure	$I_{(012)}$ (%)	$I_{(021)}$ (%)
0	0	0	fully ordered rhombohedral Gd_6UO_{12}	100	100
0.07	0.0817	0.15	partly disordered rhombohedral $Gd_6UO_{12-\delta}$	92.28	90.97
6/7	1	0	fully disordered rhombohedral Gd_6UO_{12}	44.65	36.44
6/7	1	0.86	fully disordered rhombohedral $Gd_6UO_{12-\delta}$	43.94	33.17
6/7	1	2	$Gd_6UO_{12-\delta}$ with cubic defect-fluorite structure	0	0

the intensity of superlattice reflections; compare the states with $\delta = 0$ and $\delta = 0.86$ represented by dark and light blue curves in Fig. 2. A terminating state of the order–to–disorder phase transformation in $Gd_6UO_{12-\delta}$ is its defect-fluorite structure represented by the formula Gd_6UO_{12-2} [4]. This state is a consequence of the accumulation of both the cation antisite defects and oxygen vacancies with their highest possible concentrations ($\beta_d = 6/7$ and $\delta = 2$). Correspondingly, the superlattice (012) and (021) reflections disappear entirely because of the transformation of the material from the rhombohedral structure to the cubic fluorite one. Thus, the vanishing of the superlattice peaks is due to the accumulation of both the cation antisite defects and oxygen vacancies only; no additional displacement of atoms is needed. This is in line with previously reported *qualitative* studies of the radiation-induced order–to–disorder transformations in Gd_6UO_{12}. Table 2 summarizes the evolution of the XRD superlattice peaks for $Gd_6UO_{12-\delta}$ with various β and δ parameters.

The estimated oxygen-deficiency ($\delta = 0.149(50)$) in the as-prepared $\{Gd_{5.930}U_{0.070}\}_{18f}[U_{0.917}Gd_{0.066}]_{3a}O_{11.851}$ phase is due to the presence of a small amount of U^{4+} (~ 0.105) in the sample. The majority of U^{4+} cations (0.070) is found to occupy 18f sites. This fact is logical if taking into account the similar ionic radii of U^{4+} and Gd^{3+} ions [31]. To give evidence of the presence of U^{4+} cations in the as-prepared sample we have performed the refinements of XRD data for various scenarios, taking into considerations the different scattering factors of U^{4+}, U^{5+} and U^{6+} cations [32]. If the presence of all uranium cations in 6+ valence state is considered (no U^{4+} is present), the refinements result in higher values of the goodness parameters ($R_p = 8.01\%$, $R_{wp} = 12.3\%$) in comparison with those reported in Table 1. Similarly, the refinements comprising a small amount of U^{5+} lead to worse fitting results.

In support of our findings, in addition to the refinements, we have carried out the bond valence sum (BVS) calculations [33] to estimate the oxidation states of atoms in the as-prepared $Gd_6UO_{12-\delta}$. The value of BVS for the $3a$ site is found to be 5.24. This value is in good agreement with that reported by Usman *et al.* [8]. Furthermore, the calculated BVS value is quite close to the total valence of cations on $3a$ site (~ 5.632) derived from the results of Rietveld method. It is worth to note that the presence of U^{5+} would give a larger difference between the calculated BVS and the total valence of cations on $3a$ site.

It should be noted that the existence of U^{4+} in the sample cannot be attributed to the unreacted UO_2 precursor phase. This is because this phase is excluded (the sample contains only the $Gd_6UO_{12-\delta}$ phase), when taking into account the relatively high accuracy of the quantitative XRD analysis (~ 1 wt.%). The presence of U^{4+}, *i.e.*, oxygen deficiency could also be a consequence of high-energy mechanical treatment leading to chemical *redox* processes [34]. It has been suggested that the mechanochemical reduction takes place at the surface of the milled oxide. Oxygen bonds on the cleaved oxide surfaces are broken during the mechanical treatment leading to the reduction of the sample and to a release of oxygen to the vial's internal volume. In this case, the rupture of oxide surface layers and surface stress are assumed to provide the

driving force for the reduction. In addition to the milling step of the preparation of $Gd_6UO_{12-\delta}$ phase, a partial deficit of oxygen in the free air atmosphere (in comparison to oxygen flow) during the annealing step of the sample preparation can contribute to the appearance of U^{4+} in the sample.

The analysis revealed that both 18f and $3a$ sites are six-fold coordinated. In contrast, Usman *et al.* [8] have reported the seven coordinate environment around the 18f sites for the rare earth uranates. Thus, the presence of the 18f octahedra in the as-prepared $Gd_6UO_{12-\delta}$ seems to be a striking local structural feature. However, it may be a consequence of a relatively large oxygen deficiency in the as-prepared $Gd_6UO_{12-\delta}$. Note that in the previously reported uranate structures, a six coordinate environment around the rare earth cation has also been reported [35]. The $3a$ site is symmetrically surrounded by the anions with six identical bond lengths $(U,Gd)_{3a}$–O, whereas the geometry of octahedra around the 18f site is found to be distorted. The estimated bond lengths in the material are listed in Table 1. Fig. 3 shows the rhombohedral structure of the $Gd_6UO_{12-\delta}$ crystal with the local polyhedra occupied by Gd and U ions.

This work presents the combined mechanochemical–thermal synthesis of the rhombohedral $Gd_6UO_{12-\delta}$ single phase. In contrast to the conventional thermal solid state preparations and/or solution chemistry-based routes reported previously, the processing used here represents a simple, less elaborate, solvent-free, high-yield, short processing time, and, thus, a low-cost procedure for the synthesis of this nuclear material. These advantages of the preparation of $Gd_6UO_{12-\delta}$ are consequences of an accelerated mass transfer and enhanced ionic diffusivity at contact zones between precursors due to reduced diffusion paths as a result of their mechanical preactivation. The results of Rietveld analysis of XRD data show that the as-prepared uranate exhibits a remarkable cation antisite disorder (ASD = 0.0817(8)) and a relatively high concentration of oxygen vacancies ($\delta = 0.149(50)$). The performed structural simulations for $Gd_6UO_{12-\delta}$ with various ASD reveal a decrease of the relative intensities of XRD superlattice reflections from 100%, characteristic for the fully ordered phase (ASD = 0), to about 40% for the fully disordered rhombohedral phase (ASD = 1). For the fictitious state with the highest possible cation antisite defects and oxygen vacancies (ASD = 1 and $\delta = 2$), the superlattice reflections disappear entirely because of the transformation of $Gd_6UO_{12-\delta}$ from the rhombohedral structure to the cubic fluorite one. The estimated bond lengths in the material indicate that the nonequilibrium distribution of cations does not influence the symmetrical geometry of polyhedra around the $3a$ sites, whereas the octahedra around the 18f sites are found to be distorted. The latter may be a consequence of a relatively large oxygen deficiency in the as-prepared $Gd_6UO_{12-\delta}$.

Author statement

Gaspar Darin: Conceptualization, Methodology, Software, Visualization. **Kengo Imakuma:** Investigation, Formal analysis. **Rafael Trautwein Santiago:** Visualization, Investigation. **Klebson Lucenildo Da Silva:** Conceptualization, Supervision, Formal analysis, Re-

sources, Writing - Original Draft, Writing - Review & Editing. **Luiz Fernando Cótica:** Formal analysis, Supervision. **Martin Fabián:** Investigation, Formal analysis. **Jan Valíček:** Investigation, Visualization. **Horst Hahn:** Supervision. **Vladimír Šepelák:** Supervision, Writing - Original Draft, Writing - Review & Editing.

Declaration of Competing Interest

The authors declare that they have no known competing financial interests or personal relationships that could have appeared to influence the work reported in this paper.

Acknowledgements

References

[1] M. Sahu, K. Krishnan, D. Jain, M.K. Saxena, S. Dash, Investigation on thermophysical properties of RE_6UO_{12}(s) (RE = La, Pr, Nd, Sm), Thermochim. Acta 637 (2016) 120–131.

[2] E.A. Aitken, S.F. Bartram, E.F. Juenke, Crystal chemistry of the rhombohedral $MO_3 \cdot 3R_2O_3$ compounds, Inorg. Chem. 3 (1964) 949–954.

[3] H. Jena, R. Asuvathraman, M.V. Krishnaiah, K.V.G. Kutty, X-ray powder diffraction of RE_6UO_{12} (RE = Eu, Gd, and Dy), Powder Diffr. 16 (2001) 220–223.

[4] M. Tang, K.S. Holliday, C. Jiang, J.A. Valdez, B.P. Uberuaga, P.O. Dickerson, R.M. Dickerson, Y. Wang, K.R. Czerwinski, K.E. Sickafus, Order-to-disorder phase transformation in ion irradiated uranium-bearing delta-phase oxides $RE_6U_1O_{12}$ (RE = Y, Gd, Ho, Yb, and Lu), J. Solid State Chem. 183 (2010) 844–848.

[5] H. Liu, D.Y. Yang, W. Zhang, C.G. Liu, Y. Xia, Y.H. Li, Response of the physical properties of δ-Y_6WO_{12} and Y_6UO_{12} to pressure, Comput. Mater. Sci. 134 (2017) 201–205.

[6] L.J. Chen, X. Su, J. Wen, D.Y. Yang, Y.H. Li, B.T. Hu, First-principles study of energetic and electronic properties of δ-Re_6MO_{12} (Re = Ho, Gd, Y; M = U, W), J. Appl. Phys. 114 (2013) 083714.

[7] D. Pieck, L. Desgranges, P. Matheron, H. Palancher, Evidence of a new crystalline phase in U-Gd-O phase diagram, J. Nucl. Mater. 461 (2015) 186–192.

[8] M. Usman, J. Felder, G. Morrison, H.C. zur Loye, A family of rare earth uranium oxides, $RE_6UO_{12-\delta}$, (RE = rare earth). Synthesis, structure and magnetic behavior, J. Solid State Chem. 266 (2018) 210–216.

[9] M. Tang, K.S. Holliday, J.A. Valdez, B.P. Uberuaga, P.O. Dickerson, R.M. Dickerson, Y. Wang, K.R. Czerwinski, K.E. Sickafus, Microstructural evolution in irradiated uranium-bearing delta-phase oxides $A_6U_1O_{12}$ (A = Y, Gd, Ho, Yb, and Lu), J. Nucl. Mater. 407 (2010) 44–47.

[10] M. Tang, K.S. Holliday, J.A. Valdez, B.P. Uberuaga, P.O. Dickerson, R.M. Dickerson, Y. Wang, K.R. Czerwinski, K.E. Sickafus, Radiation damage effects in the uranium-bearing δ-phase oxide $Y_6U_1O_{12}$, J. Nucl. Mater. 389 (2009) 497–499.

[11] H. Jena, R. Asuvathraman, K.V.G. Kutty, Combustion synthesis and thermal expansion measurements of the rare earth-uranium ternary oxides RE_6UO_{12} (RE = La, Nd and Sm), J. Nucl. Mater. 280 (2000) 312–317.

[12] M. Sahu, K. Krishnan, B. Kanrar, M.K. Saxena, S. Dash, Study of variation in thermophysical properties of RE_6UO_{12}(s) along the lanthanide series, J. Radioanal Nucl. Chem. 313 (2017) 487–496.

[13] M. Sahu, K. Kumari, M.K. Saxena, S. Dash, Investigation in the variation of Gibbs energy of formation of RE_6UO_{12} (RE = La, Nd, Sm, Eu, Gd, Tb, Dy, Ho, Tm, Yb, Lu) along the 4f series, J. Chem. Thermodyn. 138 (2019) 374–386.

[14] R.V. Krishnan, G. Jogeswararao, K. Ananthasivan, The standard molar enthalpies of formation of RE_6UO_{12} (RE = La, Nd) by acid solution calorimetry, J. Therm. Anal. Calorim. 121 (2015) 1375–1382.

[15] V. Šepelák, A. Düvel, M. Wilkening, K.-D. Becker, P. Heitjans, Mechanochemical reactions and syntheses of oxides, Chem. Soc. Rev. 42 (2013) 7507–7520.

[16] F. Gomollón-Bel, Ten chemical innovations that will change our world: IUPAC identifies emerging technologies in chemistry with potential to make our planet more sustainable, Chem. Int. 41 (2019) 12–17.

[17] J. Rodríguez-Carvajal, FullProf Suite, Institute Laue-Langevin, Grenoble, France, 2019.

[18] J. Wang, R.P. Sagar, H. Schmider, V.H. Smith Jr., X-ray elastic and inelastic scattering factors for neutral atoms Z = 2-92, Atomic Data Nuclear Data Tables 53 (1993) 233–269.

[19] B.E. Warren, X-Ray Diffraction, Dover Publications, Inc., New York, 1990.

[20] Inorganic Crystal Structure Database (ICSD)FIZ Karlsruhe, Leibniz Institute for Information Infrastructure, Karlsruhe, 2020.

[21] K. Momma, F. Izumi, VESTA 3 for three-dimensional visualization of crystal, volumetric and morphology data, J. Appl. Crystallogr. 44 (2011) 1272–1276.

[22] V. Šepelák, S.M. Becker, I. Bergmann, S. Indris, M. Scheuermann, A. Feldhoff, C. Kübel, M. Bruns, N. Stürzl, A.S. Ulrich, M. Ghafari, H. Hahn, C.P. Grey, K.D. Becker, P. Heitjans, Nonequilibrium structure of Zn_2SnO_4 spinel nanoparticles, J. Mater. Chem. 22 (2012) 3117–3126.

[23] M. Fabián, P. Bottke, V. Girman, A. Düvel, K.L. Da Silva, M. Wilkening, H. Hahn, P. Heitjans, V. Šepelák, A simple and straightforward mechanochemical synthesis of the far-from-equilibrium zinc aluminate, $ZnAl_2O_4$, and its response to thermal treatment, RSC Adv. 5 (2015) 54321–54328.

[24] V. Šepelák, M. Myndyk, M. Fabián, K.L. Da Silva, A. Feldhoff, D. Menzel, M. Ghafari, H. Hahn, P. Heitjans, K.D. Becker, Mechanosynthesis of nanocrystalline fayalite, Fe_2SiO_4, Chem. Commun. 48 (2012) 11121–11123.

[25] K.L. Da Silva, V. Šepelák Jr., A. Paesano, F.J. Litterst, K.-D. Becker, Structural studies of $Bi_2(Fe_xAl_{1-x})_4O_9$ solid solutions ($0.1 \leq x \leq 1.0$) prepared by a combined mechanochemical/thermal synthesis, Z. Anorg. Allg. Chem. 636 (2010) 1018–1025.

[26] V. Šepelák, S. Bégin-Colin, G.Le Caër, Transformations in oxides induced by high-energy ball-milling, Dalton Trans 41 (2012) 11927–11948.

[27] S.A.T. Redfern, R.J. Harrison, H.S.C. O'Neill, D.R.R. Wood, Thermodynamics and kinetics of cation ordering in $MgAl_2O_4$ spinel up to 1600°C from in situ neutron diffraction, Am. Mineral. 84 (1999) 299–310.

[28] Z. Wang, P. Lazor, S.K. Saxena, G. Artioli, High-pressure Raman spectroscopic study of spinel ($ZnCr_2O_4$), J. Solid State Chem. 165 (2002) 165–170.

[29] K.E. Sickafus, A.C. Larson, N.Y.M. Nastasi, G.W. Hollenberg, F.A. Garner, R.C. Bradt, Cation disorder in high dose, neutron-irradiated spinel, J. Nucl. Mater. 219 (1995) 128–134.

[30] V. Šepelák, I. Bergmann, S. Indris, A. Feldhoff, H. Hahn, K.D. Becker, C.P. Grey, P. Heitjans, High-resolution ^{27}Al MAS NMR spectroscopic studies of the response of spinel aluminates to mechanical action, J. Mater. Chem. 21 (2011) 8332–8337.

[31] R.D. Shannon, Revised effective ionic radii and systematic studies of interatomic distances in halides and chalcogenides, Acta Crystallogr. A 32 (1976) 751–767.

[32] P.J. Brown, A.G. Fox, E.N. Maslen, M.A. O'Keefe, B.T.M. Willis, Intensity of diffracted intensities, Int. Tables Crystallogr. C (2006) 554–590.

[33] O.C. Gagné, F.C. Hawthorne, Comprehensive derivation of bond-valence parameters for ion pairs involving oxygen, Acta Cryst. B71 (2015) 562–578.

[34] V. Šepelák, M. Menzel, K.D. Becker, F. Krumeich, Mechanochemical reduction of magnesium ferrite, J. Phys. Chem. B 106 (2002) 6672–6678.

[35] Y. Hinatsu, N. Masaki, T. Fujino, The crystal structure of La_6UO_{12}, J. Solid State Chem. 73 (1988) 567–571.